Supplementary Information (SI) for Soft Matter: *Jamming transition and normal modes of polydispersed soft particle packing*

Kuniyasu Saitoh[1] and Brian P. Tighe[2]

[1] *Department of Physics, Faculty of Science, Kyoto Sangyo University, Kyoto 603-8555, Japan*
[2] *Delft University of Technology, Process & Energy Laboratory, Leeghwaterstraat 39, 2628 CB Delft, The Netherlands*

(Dated: December 20, 2024)

I. ADDITIONAL RESULTS OF NUMERICAL SIMULATIONS AND NORMAL MODE ANALYSIS

In this section, we show additional results of our molecular dynamics (MD) simulations of polydispersed soft particles. We explain size distributions of the particles (Sec. I A) and examine how elastic energy and mean overlap depend on the polydispersity and packing fraction of the particles (Sec. I B). We also analyze static structures of polydispersed soft particles (Sec. I C) and show our results of participation ratio (Sec. I D).

A. Size distributions

In our MD simulations, we randomly sample each particle radius R from a power-law distribution function,

$$P(R) \propto R^{-\nu} \ . \tag{1}$$

The power-law exponent is given by $\nu = 3$ and the distribution function is defined in the range, $R_{\rm min} < R < R_{\rm max}$. Figure 1 shows the distribution functions $P(R)$, where the particle radius (horizontal axis) is scaled by the system length as R/L. The dashed line indicates the power-law, Eq. (1), and the symbols represent the size ratio defined as $\lambda \equiv R_{\rm max}/R_{\rm min}$ (as listed in the legend).

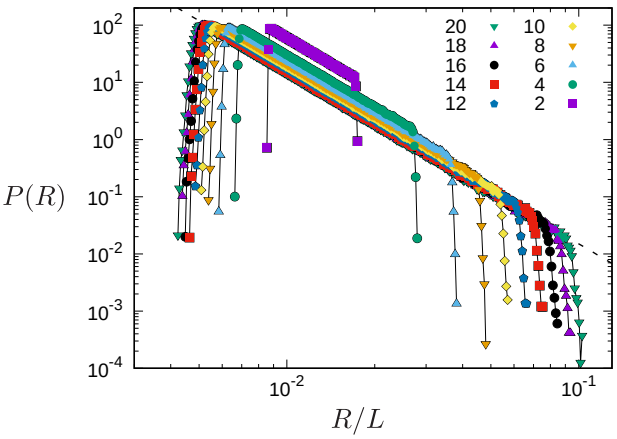

FIG. 1. Distribution functions of particle radius R, where the horizontal axis is scaled by the system length L. The size ratio, $\lambda = R_{\rm max}/R_{\rm min}$, decreases as listed in the legend. The system size (the number of particles) is $N = 2048$ and the packing fraction of the particles is given by $\phi = 0.90$. The dashed line indicates the power-law, Eq. (1).

B. Elastic energy and mean overlap

To make a static packing of polydispersed soft particles, we randomly distribute the N particles in a $L \times L$ square periodic box, where packing fraction of the particles is given by $\phi = \sum_{i=1}^{N} \pi R_i^2/L^2$. We then minimize elastic energy of the system,

$$E = \sum_{i=1}^{N} \sum_{j>i} \frac{k}{2} \delta_{ij}^2 \ , \tag{2}$$

by the FIRE algorithm, where k is the stiffness for contact forces and $\delta_{ij} > 0$ is an overlap between the particles, i and j, in contact. We stop the energy minimization if every magnitude of the force, $|\boldsymbol{f}_i|$ $(i = 1, \ldots, N)$, becomes lower than a threshold, i.e.

$$|\boldsymbol{f}_i| < 10^{-9} kL \quad \text{for} \quad \forall i \ . \tag{3}$$

Figure 2 displays a full image of a static packing of $N = 2048$ particles (after the energy minimization), where we used $\lambda = 20$ and $\phi = 0.90$. The solid lines represent a force-chain network, where their width is proportional to the magnitude of repulsive force, i.e. $k\delta_{ij}$. Figure 3 plots (a) the minimized elastic energy and (b) mean value of the overlaps δ_{ij} (after the energy minimization) as functions of ϕ, where we took ensemble averages of E and $\langle \delta \rangle$ (for each ϕ) over 1000 different configurations of the particles. The size ratio λ increases as listed in the legend of (a). As can be seen, both the elastic energy and mean overlap increase from zero at the jamming transition density, $\phi = \phi_c$, where ϕ_c shifts to higher values as the polydispersity (size ratio λ) increases.

C. Static structures

We examine the influence of polydispersity on static structures of polydispersed soft particles. Figure 4 shows

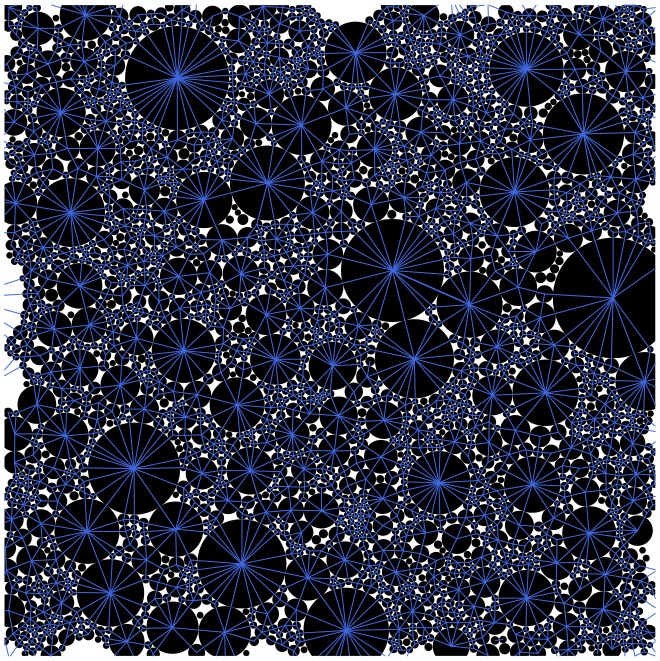

FIG. 2. A full image of a static packing of polydispersed soft particles, where the size ratio is $\lambda = 20$ and the packing fraction is $\phi = 0.90$. The solid lines represent force-chains, where their width is proportional to the magnitude of repulsive force between the particles in contact.

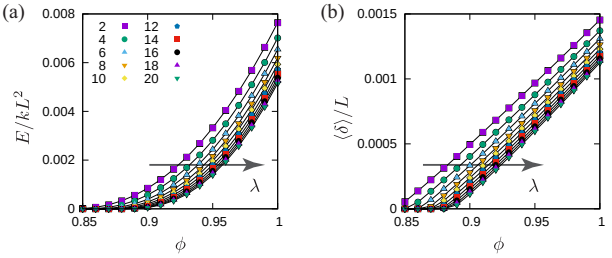

FIG. 3. (a) The scaled elastic energy E/kL^2 and (b) scaled mean overlap $\langle\delta\rangle/L$ as functions of the packing fraction ϕ. The size ratio λ increases as listed in the legend of (a) and indicated by the arrows.

radial distribution functions $g(r)$ of the particles, where λ increases as listed in the legends. In our simulations, the majority of polydisperse particles are small particles. Thus, the first peak of $g(r)$ mainly represents the contacts between two small particles. Because we fix the system length L and control the packing fraction ϕ, the smallest particle radius $R_{\rm min}$ decreases (and the largest particle radius $R_{\rm max}$ increases) with the increase of the size ratio $\lambda = R_{\rm max}/R_{\rm min}$. Therefore, as shown in Fig. 4(b), both the first and second peaks shift to shorter distances with the increase of λ. In addition, if λ is sufficiently large, the second peak of $g(r)$ almost merges with the first peak and

$$g(r) > 1$$

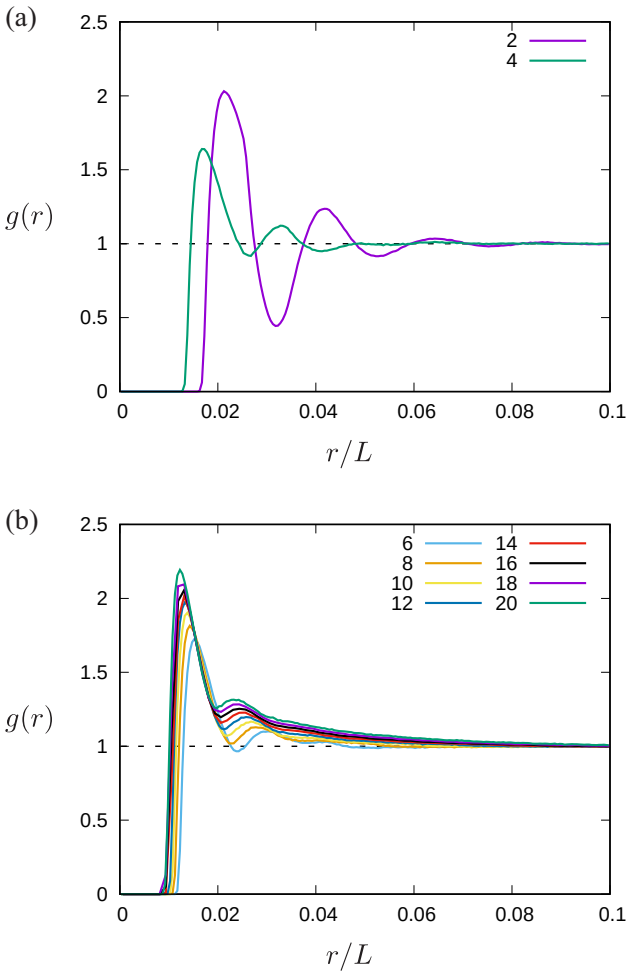

FIG. 4. Radial distribution functions of polydispersed soft particles, where the distance r is scaled by the system length as r/L (horizontal axis). The size ratio λ increases as listed in the legends.

if r is larger than the distance at the first peak (Fig. 4(b)). This means that the variation in the distance between two particles is continuous as expected in highly polydisperse systems.

In Fig. 5, we show all the data sets of (a) force distribution $P(f)$ and (b) distribution function of coordination number, $P(z)$. The force distribution with small polydispersity, e.g. with $\lambda = 2$, is well fitted to a Gaussian distribution (solid line in (a)), while one observes an exponential tail (dashed line in (a)) if the system is highly polydispersed, e.g. if $\lambda = 20$. The distribution function of coordination number broadens with the polydispersity, where the data of $\lambda = 20$ exhibits the power-law decay, $P(z) \sim z^{-4.2}$ (dashed line in (b)).

We also calculate fraction of *rattlers* as ϕ_r. Figure 6 displays ϕ_r as a function of the size ratio λ, where the packing fraction of the particles is fixed to $\phi = 0.90$. As can be seen, ϕ_r linearly increases with λ (except for the monodisperse system, $\lambda = 1$).

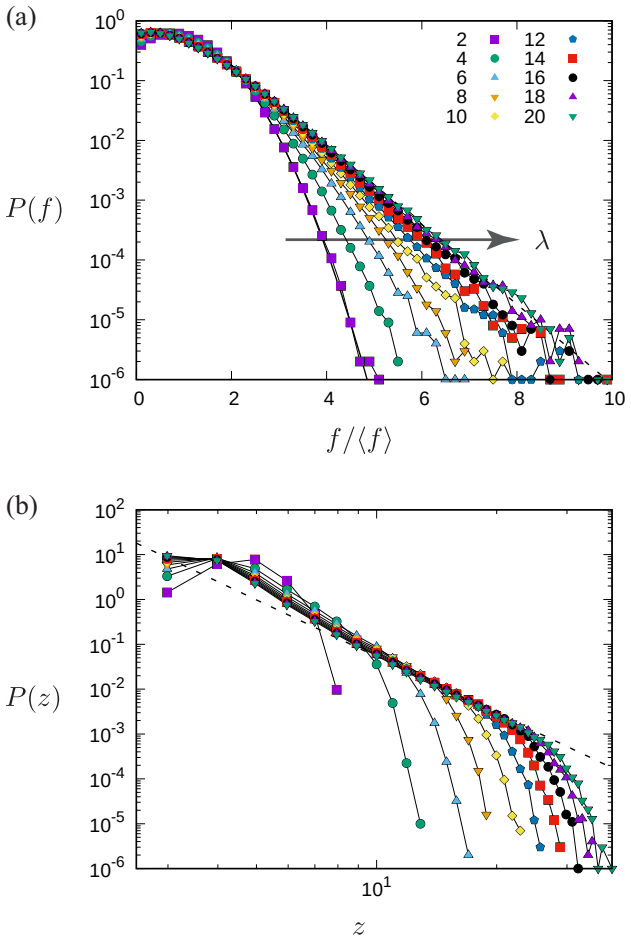

FIG. 5. (a) Semi-logarithmic plots of the distribution function of contact force f and (b) double logarithmic plots of the distribution function of coordination number z. The packing fraction of the particles is given by $\phi = 0.90$ and the size ratio λ increases as indicated by the arrow in (a) and listed in the legend of (a). In (a), f is scaled by the average $\langle f\rangle$ for each λ and the solid line is a Gaussian fit to the data of $\lambda = 2$. The dashed lines indicate (a) the exponential tail and (b) power-law decay, $P(z) \sim z^{-4.2}$, for the data of $\lambda = 20$.

D. Participation ratio

Introducing the dynamical matrix of the particles, we compute its eigenvalues and eigenvectors as λ_n and $|n\rangle$, respectively, where $n = 1, \ldots, Nd$ in $d = 2$ dimensions. We decompose $|n\rangle$ as

$$|n\rangle = (\boldsymbol{e}_{1,n}, \ldots, \boldsymbol{e}_{N,n})^{\mathrm{T}}$$

with the particle displacement, $\boldsymbol{e}_{i,n}$ $(i = 1, \ldots, N)$, associated with the n-th mode. Then, we calculate participation ratio as

$$P_r(n) = \frac{\left(\sum_{i=1}^{N} \boldsymbol{e}_{i,n}^2\right)^2}{N \sum_{i=1}^{N} |\boldsymbol{e}_{i,n}|^4} \,. \tag{4}$$

Figure 7 displays the participation ratio as a function

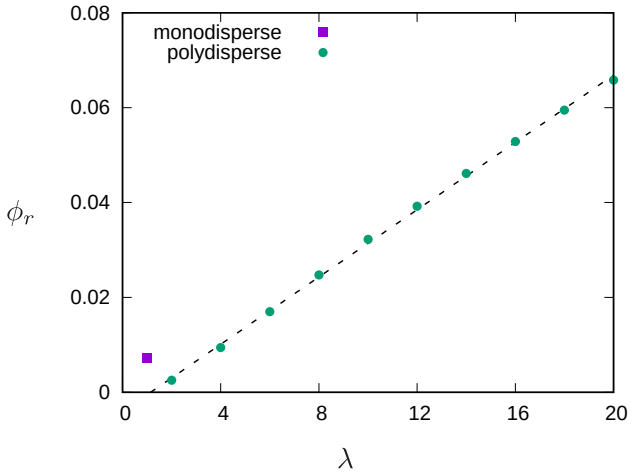

FIG. 6. The fraction of *rattlers* ϕ_r as a function of the size ratio λ, where the packing fraction of the particles is fixed to $\phi = 0.90$. The dashed line indicates a linear increase of ϕ_r.

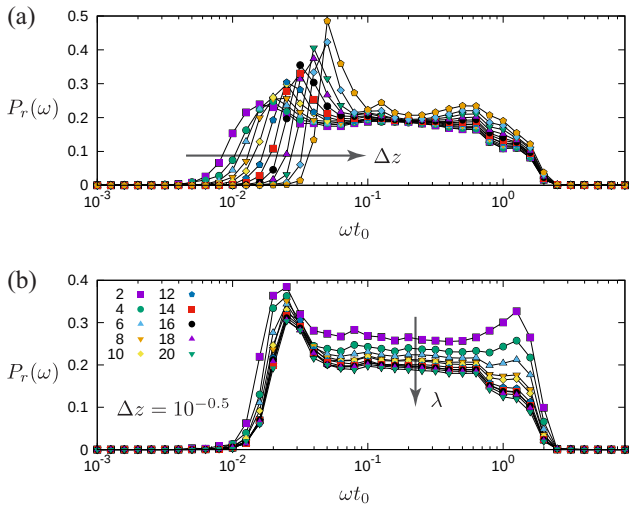

FIG. 7. (a) Semi-logarithmic plots of the participation ratio, where the size ratio is given by $\lambda = 20$. The excess coordination number increases from $\Delta z = 10^{-1}$ to $10^{0.1}$ as indicated by the arrow. (b) The dependence of participation ratio on the size ratio λ, where the excess coordination number is $\Delta z = 10^{-0.5}$. The size ratio λ increases as listed in the legend and indicated by the arrow.

of eigen-frequency ω_n, where the eigen-frequency is non-dimensionalized by the time unit, $t_0 \equiv \sqrt{m_0/k}$. As can be seen, the participation ratio depends on both (a) the distance from jamming and (b) polydispersity.

II. DYNAMICAL MATRIX AND ELASTIC MODULI

In this section, we introduce *dynamical matrix* (Hessian) and derive elastic moduli from its eigenvalues and eigenvectors. First, we show explicit forms of the dynam-

ical matrix (Sec. II A). Next, we introduce a constitutive relation (Sec. II B) and the *extended Hessian* (Sec. II C) for isotropic (de)compression. Then, we formulate the elastic moduli (Sec. II D).

A. Dynamical matrix

The $2N \times 2N$ dynamical matrix (Hessian) $\mathcal{H}$ consists of second derivatives of the elastic energy E (Eq. (2)) with respect to the particle positions, $\boldsymbol{r}_i = (x_i, y_i)$, as

$$\mathcal{H} = \begin{pmatrix} \frac{\partial^2 E}{\partial x_i \partial x_j} & \frac{\partial^2 E}{\partial x_i \partial y_j} \\ \frac{\partial^2 E}{\partial y_i \partial x_j} & \frac{\partial^2 E}{\partial y_i \partial y_j} \end{pmatrix}_{i,j=1,\ldots,N} . \tag{5}$$

We rewrite the elastic energy (Eq. (2)) as the sum of pairwise potentials as

$$E = \sum_{i=1}^{N} \sum_{j>1} e_{ij} \ , \tag{6}$$

where each potential is defined as $e_{ij} \equiv k\delta_{ij}^2/2$ ($\delta_{ij} > 0$). The second derivatives of e_{ij} are given by

$$\frac{\partial^2 e_{ij}}{\partial x_i \partial x_i} = k\left(1 - a_{ij} n_{ijy}^2\right) \ , \tag{7}$$

$$\frac{\partial^2 e_{ij}}{\partial x_i \partial y_i} = k a_{ij} n_{ijx} n_{ijy} \ , \tag{8}$$

$$\frac{\partial^2 e_{ij}}{\partial y_i \partial y_i} = k\left(1 - a_{ij} n_{ijx}^2\right) \ , \tag{9}$$

where we introduced a factor as

$$a_{ij} \equiv 1 + \frac{\delta_{ij}}{r_{ij}}$$

and $\boldsymbol{n}_{ij} \equiv \boldsymbol{r}_{ij}/r_{ij} = (n_{ijx}, n_{ijy})$ is a unit vector parallel to the relative position between the particles, i and j, in contact. Note that the second derivatives with different indexes ($i \neq j$) satisfy the following relation,

$$\frac{\partial^2 e_{ij}}{\partial \alpha_i \partial \beta_j} = -\frac{\partial^2 e_{ij}}{\partial \alpha_i \partial \beta_i} \qquad (\alpha, \beta = x, y) \ . \tag{10}$$

Each element in Eq. (5) is constructed from Eqs. (6)-(10).

B. Constitutive relation

If isotropic (de)compression is applied to an elastic body in d-dimension, strain tensor is written as

$$\epsilon_{\alpha\beta} = \frac{\epsilon}{d}\delta_{\alpha\beta} \ , \tag{11}$$

where $\epsilon \ll 1$ represents a small strain. We introduce stress tensor and bulk modulus as $\sigma_{\alpha\beta}$ and B, respectively, such that constitutive relation is given by

$$\epsilon_{\alpha\alpha} = \frac{1}{dB}\sigma_{\alpha\alpha} \ . \tag{12}$$

Here, the Einstein summation convention has been used for the subscript α. The confining pressure is defined as

$$p \equiv -\frac{1}{d}\sigma_{\alpha\alpha}$$

so that Eq. (12) is rewritten as

$$p = -B\epsilon_{\alpha\alpha} = -B\epsilon \ . \tag{13}$$

C. The extended Hessian

We assume that the system consisting of N soft particles in $d = 2$ dimensions is initially in mechanical equilibrium. If we apply the strain, Eq. (11), to the system, every particle exhibits affine displacement. Because force balance is broken by the affine displacements, the particles start to move. After the system relaxes to a static state, every contact force is balanced again, where particle displacements are now given by the sum of affine and *non-affine displacements*. We write the non-affine displacement of the i-th particle as $\delta\boldsymbol{u}_i$ and introduce a $dN = 2N$ dimensional vector as

$$|\delta\boldsymbol{u}\rangle \equiv (\delta\boldsymbol{u}_1, \ldots, \delta\boldsymbol{u}_N)^{\mathrm{T}} \ .$$

We combine the force balance equation (after the relaxation) and the constitutive relation as

$$\begin{aligned} \begin{pmatrix} |\boldsymbol{0}\rangle \\ V\Delta p/2 \\ V\Delta p/2 \end{pmatrix} &= -\begin{pmatrix} \mathcal{H} & |\Xi_{xx}\rangle & |\Xi_{yy}\rangle \\ \langle\Xi_{xx}| & \psi_{xx}^{(1)} & \psi_{yy}^{(1)} \\ \langle\Xi_{yy}| & \psi_{xx}^{(4)} & \psi_{yy}^{(4)} \end{pmatrix} \begin{pmatrix} |\delta\boldsymbol{u}\rangle \\ \epsilon/2 \\ \epsilon/2 \end{pmatrix} \\ &\equiv -\mathcal{H}_{\mathrm{ex}} \begin{pmatrix} |\delta\boldsymbol{u}\rangle \\ \epsilon/2 \\ \epsilon/2 \end{pmatrix} \ . \end{aligned} \tag{14}$$

Here, $|\boldsymbol{0}\rangle$ is the $2N$ dimensional zero vector and $\mathcal{H}$ is the dynamical matrix (Sec. II A). In addition, $\Delta p \equiv p - p_0$ with the initial pressure p_0 (before deformation) is the increment of confining pressure. We also introduced the system volume (area) and *extended Hessian* as V and $\mathcal{H}_{\mathrm{ex}}$, respectively. In Eq. (14), the two elements are identical, $\psi_{yy}^{(1)} = \psi_{xx}^{(4)}$, so that the extended Hessian $\mathcal{H}_{\mathrm{ex}}$ is a real symmetric matrix.

D. Bulk modulus

If we rewrite the $dN + 2 = 2N + 2$ dimensional vectors in the force balance equation (14) as

$$\begin{pmatrix} |\delta\boldsymbol{u}\rangle \\ \epsilon/2 \\ \epsilon/2 \end{pmatrix} \equiv |q, \epsilon/2, \epsilon/2\rangle \ ,$$

$$\begin{pmatrix} |\boldsymbol{0}\rangle \\ V\Delta p/2 \\ V\Delta p/2 \end{pmatrix} \equiv \frac{\Delta p}{2} V\,|0, 1, 1\rangle \ ,$$

Eq. (14) is written as

$$\mathcal{H}_{\rm ex}\,|q,\epsilon/2,\epsilon/2\rangle = -\frac{\Delta p}{2}V\,|0,1,1\rangle \ . \tag{15}$$

In addition, the strain is given by an inner product,

$$\epsilon = \langle 0,1,1\,|q,\epsilon/2,\epsilon/2\rangle \ . \tag{16}$$

We expand the vector, $|q,\epsilon/2,\epsilon/2\rangle$, into the series as

$$|q,\epsilon/2,\epsilon/2\rangle = \sum_{n=1}^{2N+2} a_n|n\rangle \ , \tag{17}$$

where $|n\rangle$ is the eigenvector of the extended Hessian and a_n is introduced as a coefficient. Then, substituting Eq. (17) into (15), we find

$$\sum_{n=1}^{2N+2} a_n\mathcal{H}_{\rm ex}|n\rangle = -\frac{\Delta p}{2}V\,|0,1,1\rangle \ . \tag{18}$$

Multiplying the left eigenvector $\langle n|$ to Eq. (18), we find

$$a_n\langle n|\mathcal{H}_{\rm ex}|n\rangle = -\frac{\Delta p}{2}V\langle n\,|0,1,1\rangle \ . \tag{19}$$

Because the eigenfrequency ω_n is given by

$$\langle n|\mathcal{H}_{\rm ex}|n\rangle = \omega_n^2 \ ,$$

Eq. (19) is rewitten as

$$a_n\omega_n^2 = -\frac{\Delta p}{2}\Lambda_n \ ,$$

where we have introduced $\Lambda_n \equiv V\langle n\,|0,1,1\rangle$. Therefore, the coefficient for the expansion is given by

$$a_n = -\frac{\Lambda_n}{2\omega_n^2}\Delta p \ . \tag{20}$$

Substituting Eq. (17) into (16), we find that the strain is given by

$$\begin{aligned}\epsilon &= \sum_{n=1}^{2N+2} a_n\langle 0,1,1|n\rangle \\ &= \frac{1}{V}\sum_{n=1}^{2N+2} a_n\Lambda_n^* \\ &= -\frac{\Delta p}{2V}\sum_{n=1}^{2N+2}\frac{|\Lambda_n|^2}{\omega_n^2} \ ,\end{aligned}$$

where we used Eq. (20). Therefore, from the constitutive relation, Eq. (13), the inverse of bulk modulus is given by

$$\begin{aligned}\frac{1}{B} &= \frac{1}{2V}\sum_{n=1}^{2N+2}\frac{|\Lambda_n|^2}{\omega_n^2} \\ &\sim \int_0^\infty \frac{|\Lambda(\omega)|^2}{\omega^2}D(\omega)d\omega \ ,\end{aligned} \tag{21}$$

where $D(\omega)$ is the vibrational density of states (VDOS). We use our numerical data of $|\Lambda(\omega)|^2$ and $D(\omega)$ to calculate B from Eq. (21).